HHS Public Access

Author manuscript

J Comput Assist Tomogr. Author manuscript; available in PMC 2022 June 03.

Published in final edited form as:

J Comput Assist Tomogr. 2020 ; 44(4): 511–518. doi:10.1097/RCT.0000000000001049.

Differentiation of Focal-type Autoimmune Pancreatitis from Pancreatic Ductal Adenocarcinoma Using Radiomics Based on Multi-phasic Computed Tomography

Linning E[1,$], **Yan Xu**[3,$], **Zhifeng Wu**[1], **Li Li**[4], **Na Zhang**[1], **Hao Yang**[2], **Lawrence H. Schwartz**[2], **Lin Lu**[2,*], **Binsheng Zhao**[2]

[1.]Department of Radiology, Shanxi DAYI Hospital, 99 Longcheng Street, Taiyuan, Shanxi, 10032, China

[2.]Department of Radiology, Columbia University Medical Center, 622 West 168th Street, New York, NY, 10032, USA

[3.]Department of Radiology, Beijing Friendship Hospital, Capital Medical University, Beijing, 100050, China

[4.]Department of Pathology, Shanxi DAYI Hospital, 99 Longcheng Street, Taiyuan, Shanxi, 10032, China

Abstract

Objectives—To develop radiomics model for differential diagnosis of focal-type autoimmune pancreatitis (AIP) from pancreatic ductal adenocarcinoma (PDA).

Methods—A total of 96 patients, 45 AIP and 51 PDA, were retrospectively collected. All patients underwent pretreatment abdominal CT imaging acquired at non-contrast, arterial, and venous phases. 1160 radiomics features were extracted from each phasic image to build radiomics models. The performance of radiomics model was evaluated by sensitivity, specificity, and accuracy. The results of radiomics model were also compared with those of radiologists' visual assessments.

Results—The sensitivity, specificity, and accuracy of the optimal radiomics model were 93.3%, 96.1%, and 94.8%, respectively. They were higher than those of the radiologists' assessments with sensitivity of 57.78% / 73.33%, specificity of 88.24 / 90.20%, and accuracy of 75.00% / 81.25%.

Conclusion—Radiomics is helpful for differential diagnosis of AIP in clinical practice as a noninvasive and quantitative method.

Keywords

Autoimmune pancreatitis; Pancreatic ductal adenocarcinoma; Multi-phase Computed Tomography; Radiomics

[*]Whom correspondence should be addressed to.: Lin Lu, Ph.D., Department of Radiology, Columbia University Medical Center, 622 West 168th Street, New York, NY, 10032, USA, Tel: 1 (646) 808-9216, ll2860@cumc.columbia.edu.

[$]Whom contributed equally to the work.

Declarations of interest: NO.

Introduction

Autoimmune pancreatitis (AIP) was first described by Yoshida[1] in 1995. According to the International Consensus Diagnostic Criteria (ICDC), there are two types of AIP: Type - 1 and Type - 2[2]. Type 1 AIP is a systemic disease and is the pancreatic manifestation of IgG4-related systemic disease, is more common and seen generally in Asian populations. Type 2 AIP is confined to the pancreas. The intensity of the periductal inflammatory infiltrate and the presence of ductal neutrophilic abscesses are features that assist in distinguishing type 2 AIP from chronic pancreatitis [3, 4]. Contrast-enhanced computed tomography (CECT) remains the first-line imaging modality for the evaluation of patients with suspected pancreatic disease. A diffuse sausage-shaped or focal enlargement of the pancreas with delayed enhancement or capsule-like rim enhancement on CECT is considered to be the typical sign of AIP [2]. However, the definitive diagnosis often remains challenging, particularly when AIP is accompanied by a focal pancreatic mass and abnormal enhancement. Clinically, given the rarity of AIP, the presence of a focal mass in the pancreas is often suspected to be pancreatic ductal adenocarcinoma (PDA). A 3–43% incidence of pancreatic resection for misdiagnosed PDA with a diagnosis of AIP made at surgical pathologic examination was observed [5–7]. In clinical practice, although endoscopic-ultrasound-guided fine-needle-aspiration biopsy (EUS-FNAB) is useful for diagnosing AIP, it is an invasive procedure and conclusive diagnosis of AIP is often difficult owing to the small size of specimens obtained by EUS-FNAB [8].

Numerous imaging strategies have been employed to diagnose AIP noninvasively on the basis of imaging features[6, 9–17]. To date, a major drawback of this type of methods is that all image features are described subjectively by a radiologist. As a result, the diagnostic accuracy will depend on the knowledge and analytical skill of individual radiologist. Thus, objective and quantitative diagnostic methods are urgently needed for improved diagnosis of AIP, especially focal-type AIP.

Radiomics is a form of image analysis that uses quantitative textural information, known as image features, to evaluate medical images. Radiomics is currently gaining increasing attention in oncology research and has been applied to cancer diagnosis, prognosis and treatment response assessments[18]. Well-developed radiomic features may serve as “virtual biopsy” derived biomarkers that are non-invasive, quantitative, and reproducible.

In this study, we retrospectively reviewed CT imaging data from a cohort of 45 patients with AIP and 51 patients with PDA. We evaluated the performances of retrospective radiologist assessment and radiomics methods to differentiate AIP from PDA. We aimed to evaluate whether radiomics can help improve the diagnosis of AIP.

Materials and Methods

The Institutional Review Board approved the retrospective collection and analysis of the study data, and the need for informed consent from patients was waived.

Patient Selection

Between January 2012 and May 2019 we searched the clinical and radiological databases of two institutions to identify patients with focal-type AIP. A total of 56 patients had been diagnosed with focal-type AIP (Type 1). Among the 56 patients, 11 of them were excluded due to missing of contrast-enhancement CT images. Finally, a total of 45 patients with focal-type AIP (Type 1) were used for study, including 14 patients confirmed with histologic diagnosis and 31 patients met the ICDC. For the 14 histologically confirmed patients, one was confirmed with specimens from pancreaticoduodenectomy, two were confirmed with distal pancreatectomy, and 11 were confirmed with endoscopic-ultrasound–guided core-needle biopsy. For the ICDC, it included five cardinal features of AIP including parenchymal imaging, ductal imaging, serology, other organ involvement, histology of pancreas and response to steroid therapy. Each criterion was further classified into two levels (levels 1 and 2). The data flow chart for collecting AIP was presented in Fig. 1.

Patients with PDA were randomly selected from our institutional radiological database. In terms of distribution of age and sex, the PDA group was matched to the patients with AIP.

The inclusion criteria of focal-type AIP were as follows: 1) patients underwent pretreatment triple-phase pancreatic CT; and 2) definitive diagnosis was made by surgical resection, EUS-FNAB, or meeting the ICDC. Conversely, cases were excluded for the following reasons: 1) CT findings of distant metastasis in patients with PDA; 2) patients had received treatment for the pancreatic lesion before CT examination; and 3) image quality was unsatisfactory due to severe artifacts.

Image Acquisition

Patients were imaged on a range of helical multidetector (16, 64, 128 and 256 slices) CT scanners. After an unenhanced scanning (kVp 120, mAs 100–500), dual-phase (arterial and venous) of the upper abdomen imaging was acquired using an intravenous bolus injection of iodinated contrast (1 mL/kg) with a 3 – 4 mL/sec injection rate; the imaging of arterial phase acquisition was triggered by bolus tracking upon the aorta (Trigger cutoff on aorta is 100 HU. Generally, the triggering of scanning is 35–45s after the injection start when pancreatic parenchyma could reach the maximum enhancement). The imaging of the venous phase was acquired at the 60 s delay after the injection. All CT images were reconstructed with a slice thickness that varied from 1~5 mm.

Retrospective Radiologist Assessment and CT Sign Evaluation

CT images of each patient were reviewed by two radiologists (Z.N. and W.Z. with 6 and 10 years of experience in the interpretation of abdominal imaging). They were blinded to the final diagnosis but aware that the study cohort included patients with AIP and PDA. A checklist of the CT signs (Table 3) collected from the previous literature on AIP and PDA was provided for the radiologists' interpretation[2, 9–12, 14–17, 19–21]. They independently interpreted triple-phase CT signs on each patient and made their own diagnosis. If the two independent interpretations disagreed, a consensus interpretation was made for each patient in disagreement.

Region of Interest (ROI) Delineation

The lesion ROI delineation was performed by one radiologist (E.L. with 16 years of experience in the interpretation of abdominal imaging and blinded to the final diagnosis), using an in-house imaging platform (Weasis)[22] under an abdominal window/level setting (Window: 350 HU; Level: 50 HU). For obtaining the ROIs on the triple phases in each patient, an ROI on the arterial-phase was first delineated and then copied to non-enhanced and venous phase images. Limited modifications were made only if large organ movement existed. The vessels were excluded from the delineated lesion ROI.

Feature Extraction and Reproducibility Assessment

For each delineated lesion ROI, 1160 well-defined quantitative image features were extracted using an in-house feature extraction software package implemented on MATLAB 2016b (MathWorks, Natick, USA). The 1160 image features were an extension of a set of the 89 image features published in a previous radiomics study by expanding the scales of some feature parameters. The details of each feature can be found in [23].

To assess the interobserver agreement for the computation of the radiomic features, we randomly chose a subset of 40 patients (20 AIPs and 20 PDAs) from the entire patient list and asked a second radiologist (10 years of experience in the interpretation of abdominal imaging and blinded to the final diagnosis) to delineate the lesion ROIs and extract the features in the same manner and using the same software tools. The concordance correlation coefficient (CCC) was used to indicate the reproducibility of the radiomics features[24].

Radiomics Model Building

To capture informative image information as much as possible, we extracted 1160 features to quantify phenotypic characteristics of lesions at three CT phases. However, analyzing such a large feature set was difficult and prone to overfitting on data. Therefore, a novel coarse-to-fine two-stage strategy was adopted[25, 26]. At the coarse-stage, considerably numbers of redundant features were removed from the feature set based on the minimum Redundancy Maximum Relevance algorithm[27]. At the fine-stage, a compact set of informative and nonredundant features were combined using the Random Forest (RF) algorithm[28]. More detailed description on radiomics model building are presented in the Appendix.

Machine-learning algorithms were coded using the Matlab 2018a (Mathworks, Natick, USA) package. In the RF algorithm, we took the default values for all of the algorithm's parameters except the "Number of Tree" and "Minimal Leaf Size". These two parameters could regularize the fitness power of RF and help prevent overfitting, which was especially useful for studying small datasets like ours. In this work, we empirically set the "Number of Tree"=15 (approximately 15% of total data) and "Minimal Leaf Size"= 10 (approximately 10% of total data).

Models Based on Triple-phase CT Imaging

Four radiomics models, i.e., a noncontrast model, an arterial model, a venous model, and a hybrid model, were constructed in our study. The noncontrast, arterial, and venous models

were independently built based on each of the three-phase CT images, whereas the hybrid model was built on the average prediction of the three-phase models.

Performance Evaluation and Statistical Analysis

For the radiologist's assessment, accuracy, sensitivity, specificity, negative predictive value and positive predictive value were used to indicate performance. For the radiomics prediction model, sensitivity, specificity, and the AUC (the area under the receiver operating characteristic curve (ROC)) was used. The AUC was calculated through five-fold cross-validation.

The significant difference for continuous data and categorical data were evaluated using the Student *t*-test and the chi-squared test, respectively. The tests were performed on SPSS, version 19.0 (SPSS, IL, USA), and $p < 0.05$ was considered significantly different.

Results

Patient Demographics

A total of 96 patients – including 45 patients with focal-type AIP and 51 patients with PDA – were evaluated. No significant difference was found among the patients between the two cohorts in terms of age ($p = 0.142$) and gender ($p = 0.083$). More details of the patient demographics and clinical features are summarized in Table 1.

Retrospective Radiologist Assessment

As shown in Table 2, radiologist 1 correctly diagnosed 26 AIP and 46 PDA with 75.00% accuracy. Radiologist 2 diagnosed 33 AIP and 45 PDA with 81.25% accuracy.

CT Sign Evaluation

The frequencies of all the CT signs of patients with AIP and PDA are summarized in Table 3. Capsule-like rim enhancement and homogeneous enhancement in the venous phase are the two typical CT signs for AIP diagnosis (Fig. 2). On all three phases, the mean CT attenuation values of pancreatic involvement were significantly higher in AIP than in PDA. ($p < 0.001$, Table 1).

Renal involvement was more frequent in patients with AIP than those with PDA ($p = 0.020$). Renal involvement in our study indicated the CT sign that, CT images revealed a bilateral diffuse renal swelling with multiple hypodense lesions, and bilateral focal thinning or absence of the renal cortex. Some patients showed diffuse thickening of the renal pelvis wall. Vascular involvement was more frequent in PDA than in AIP ($p = 0.027$). No difference was noted between these two cohorts in the frequency of lymphadenopathy, biliary dilatation, or retroperitoneal stranding or fibrosis.

Radiomics Prediction Model

To build the four radiomics models, we extracted three radiomics feature sets, each containing 1160 features, from the three-phase CT images separately. For each feature set, we applied a CCC threshold of 0.60 to screen features with low reproducibility. As

a result, there were 714, 726 and 694 reproducible features remained in each set. The radiomics models based on the reproducible features and the coarse-to-fine strategy were developed to output the probability of being AIP or PDA. Finally, a hybrid model was built by averaging the output probabilities of the three single-phase models. The performances of the hybrid radiomics model achieved AUC (95% CI) of 0.977 (0.924, 0.997). The ROCs of the four radiomics models are presented in Fig. 3. The features selected to create radiomics model as well as their importance to the model (the predictor importance output by the RF algorithm) are listed in Table 4. The “LongRun-Low-GrayLevel-Emphasis” and “LongRun-High-GrayLevel-Emphasis” features were the radiomic features most important to our models built to distinguish AIP from PDA.

Discussion

Based on the triple-phase CT imaging, we developed four radiomics models. Among them, the hybrid model demonstrated the highest performance of AUC = 97.7% and accuracy = 94.80% for distinguishing focal-type AIP from PDA. Our results indicated that radiomics analysis could serve as a noninvasive, quantitative and potentially useful tool for improving the diagnostic accuracy of focal-type AIP in clinical practice.

The retrospective diagnostic accuracy assessments of the two radiologists were 75% and 81.25%. This result is similar to that of a previous study in which the accuracy for diagnosing AIP was reported between 53% and 78%[14]. Noticeably, the radiomics models showed improved diagnostic performance than the radiologists (Table 2). Even based on noncontrast CT imagine, the radiomics model shows a diagnostic accuracy of 79.19%. A possible explanation for the low and varied diagnostic accuracy of radiologists was that the identification of the specific CT signs was subjective and relied on the experience of the radiologists. Moreover, a low agreement between the two radiologists was found for the specific CT signs of AIP[14, 15].

Compared to radiologists’ subjective evaluation, radiomics models can enable the quantitative assessment of heterogeneity information for AIP and PDA on CT imaging, which may be reflected by their heterogeneous nature at the gross and cellular levels based on different pathological features[3, 4, 29]. As can be seen from Fig 4, PDA shows the haphazard arrangement of neoplastic cells and fibrous connective tissue. However, AIP shows significant lymphoplasmacytic infiltration around atrophic pancreatic pancreatic ducts with fibrosis, such differences in pathology are likely to be reflected on imaging as differences in heterogeneity. However, these pathological features are difficult to detect with the naked eye. In our study, as shown in Table 4, aside from the features to characterize homogeneity information, such as the above-mentioned “Run-Length” features, the features to characterize heterogeneity information such as “LoG” (Laplacian of Gaussian)[30] and “GLCM” (Gray Level Co-Occurrence Matrix)[31] features, were also involved. The “LoG” and “GLCM” are features that have been proven useful in predicting the pathological features of certain tumor types[32–35]. Therefore, the quantification of such features could potentially serve as imaging biomarkers for supporting precise diagnoses for AIP.

Moreover, our study showed that CECT has a definitive impact on the selection of radiomics features. As shown in Table 4, the three radiomics models are built on different features. The underlying reason for the variability of radiomics features may be correlated with the biological heterogeneity within the tumor tissue (vascularity or lack of it). The heterogeneity on CT can be quantified using radiomics analysis, which reflects the coarseness and regularity that result from local spatial variations in image brightness (an extension from measuring attenuation). Therefore, our study indicated that radiomics features may be affected by the phase (arterial or venous) of acquisition and some scan-related parameters (i.e. contrast dose and injection rate), and the reproducibility of radiomics features due to image acquisition should be investigated extensively before using these features in clinical practice.

Our study has a major limitation, i.e., we were only able to examine a small number of patients due to the rarity of the AIP disease. Future studies with a larger patient population in multiple institutions are needed for the validation of the developed radiomics models.

Conclusion

Our results show that radiomics, as a noninvasive and quantitative method, has a great potential to improve the accuracy of AIP diagnosis.

Acknowledgments

This work was supported by the Natural Science Foundation of Shanxi Province, China. [Grant number 201701D121151].

Appendix

Radiomics Model Building

A ‘coarse’ to ‘fine’ two-stage strategy was developed to screen redundant and non-informative features and create a compact set of the informative and non-redundant features for model building.

Within the two-stage strategy, the first stage coarse selection was consisted of two sub-procedures, the unsupervised hierarchical clustering and the feature ranking. The unsupervised hierarchical clustering was performed in three steps. Firstly, calculate correlation between features; secondly, organize all features into a hierarchical clustering tree according to their mutual correlations; finally, by setting a correlation threshold, all features were separated into a series of redundant feature groups (i.e. when setting correlation threshold as 0.5, it means all candidate features are clustered into a series of redundant feature groups, within which mutual correlation of all feature exceed 0.5). For each group of redundant features, only the most informative features were kept, and others were excluded. In the feature ranking procedure, the minimum Redundancy Maximum Relevance (mRMR) algorithm (1) were applied to rank the correlated features. The top-ranked feature was selected as the most informative feature for each redundant feature group. In our study, by setting a high correlation threshold, a compact candidate feature list can be attained after the coarse selection.

At the second stage, the fine selection was consisted of two algorithms, the Incremental Forward Search (IFS) (1) and the Random Forest algorithm (2). IFS was adopted to evaluate features sequentially. In our study, up to twenty features (top 20 features identified in the ranking step, empirically set to 20% of the patient data) were evaluated. IFS initiated on an empty set and included k features if and only if the addition of the k features could increase the performance of the classification models. The procedure of IFS was repeated until all the candidate features in the compact candidate feature list were evaluated (The forward step k was set as 3 in our study). During the IFS, the RF algorithm was used to combine features. Thus, totally 20/3=6 candidate models were created during the IFS. The final optimal model was determined as the model that could achieve the best performance in terms of area under a receiver operating characteristic curve (AUC) which was estimated by five-fold cross-validation.

All the algorithms for model building were implemented on the platform of Matlab 2017b (Mathworks, Natick, USA). Parameters for the mRMR and RF algorithms were all set as default.

List of all abbreviations

AIP	autoimmune pancreatitis
PDA	pancreatic ductal adenocarcinoma
ICDC	International consensus diagnostic criteria
CECT	Contrast-enhanced computed tomography
EUS-FNAB	Endoscopic-ultrasound-guided fine-needle-aspiration biopsy
ROI	Region of interest
CCC	Concordance correlation coefficient
ROC	Receiver operating characteristic curve
AUC	Area under the receiver operating characteristic curve

Reference

1. Yoshida K, Toki F, Takeuchi T, et al. Chronic pancreatitis caused by an autoimmune abnormality. Proposal of the concept of autoimmune pancreatitis. Dig Dis Sci 1995; 40:1561–1568 [PubMed: 7628283]
2. Shimosegawa T, Chari ST, Frulloni L, et al. International consensus diagnostic criteria for autoimmune pancreatitis: guidelines of the International Association of Pancreatology. Pancreas 2011; 40:352–358 [PubMed: 21412117]
3. Kloppel G, Sipos B, Zamboni G, et al. Autoimmune pancreatitis: histo- and immunopathological features. J Gastroenterol 2007; 42 Suppl 18:28–31 [PubMed: 17520220]
4. Zen Y The Pathology of IgG4-Related Disease in the Bile Duct and Pancreas. Semin Liver Dis 2016; 36:242–256 [PubMed: 27466794]
5. de Castro SM, de Nes LC, Nio CY, et al. Incidence and characteristics of chronic and lymphoplasmacytic sclerosing pancreatitis in patients scheduled to undergo a pancreatoduodenectomy. HPB (Oxford) 2010; 12:15–21 [PubMed: 20495640]

6. Wang J, Su T, Jia N, et al. Computed tomographic and magnetic resonance imaging presentations of pancreatitis maldiagnosed as pancreatic carcinoma. Pancreas 2010; 39:262–264 [PubMed: 20182308]
7. van Heerde MJ, Biermann K, Zondervan PE, et al. Prevalence of autoimmune pancreatitis and other benign disorders in pancreatoduodenectomy for presumed malignancy of the pancreatic head. Dig Dis Sci 2012; 57:2458–2465 [PubMed: 22588243]
8. Mizuno N, Bhatia V, Hosoda W, et al. Histological diagnosis of autoimmune pancreatitis using EUS-guided trucut biopsy: a comparison study with EUS-FNA. J Gastroenterol 2009; 44:742–750 [PubMed: 19434362]
9. Sahani DV, Kalva SP, Farrell J, et al. Autoimmune pancreatitis: imaging features. Radiology 2004; 233:345–352 [PubMed: 15459324]
10. Manfredi R, Graziani R, Cicero C, et al. Autoimmune pancreatitis: CT patterns and their changes after steroid treatment. Radiology 2008; 247:435–443 [PubMed: 18430876]
11. Sahani DV, Sainani NI, Deshpande V, et al. Autoimmune pancreatitis: disease evolution, staging, response assessment, and CT features that predict response to corticosteroid therapy. Radiology 2009; 250:118–129 [PubMed: 19017924]
12. Kamisawa T, Takuma K, Anjiki H, et al. Differentiation of autoimmune pancreatitis from pancreatic cancer by diffusion-weighted MRI. The American journal of gastroenterology 2010; 105:1870 [PubMed: 20216538]
13. Manfredi R, Frulloni L, Mantovani W, et al. Autoimmune pancreatitis: pancreatic and extrapancreatic MR imaging–MR cholangiopancreatography findings at diagnosis, after steroid therapy, and at recurrence. Radiology 2011; 260:428–436 [PubMed: 21613442]
14. Zaheer A, Singh VK, Akshintala VS, et al. Differentiating autoimmune pancreatitis from pancreatic adenocarcinoma using dual-phase computed tomography. J Comput Assist Tomogr 2014; 38:146–152 [PubMed: 24424563]
15. Furuhashi N, Suzuki K, Sakurai Y, et al. Differentiation of focal-type autoimmune pancreatitis from pancreatic carcinoma: assessment by multiphase contrast-enhanced CT. Eur Radiol 2015; 25:1366–1374 [PubMed: 25433412]
16. Lee-Felker SA, Felker ER, Kadell B, et al. Use of MDCT to Differentiate Autoimmune Pancreatitis From Ductal Adenocarcinoma and Interstitial Pancreatitis. AJR Am J Roentgenol 2015; 205:2–9 [PubMed: 26102377]
17. Negrelli R, Manfredi R, Pedrinolla B, et al. Pancreatic duct abnormalities in focal autoimmune pancreatitis: MR/MRCP imaging findings. European radiology 2015; 25:359–367 [PubMed: 25106489]
18. Lubner MG, Smith AD, Sandrasegaran K, et al. CT Texture Analysis: Definitions, Applications, Biologic Correlates, and Challenges. Radiographics 2017; 37:1483–1503 [PubMed: 28898189]
19. Takahashi N, Kawashima A, Fletcher JG, et al. Renal involvement in patients with autoimmune pancreatitis: CT and MR imaging findings. Radiology 2007; 242:791–801 [PubMed: 17229877]
20. Dite P, Nechutova H, Uvirova M, et al. Autoimmune pancreatitis. Biomed Pap Med Fac Univ Palacky Olomouc Czech Repub 2014; 158:17–22 [PubMed: 24572485]
21. Madhani K, Farrell JJ. Autoimmune Pancreatitis: An Update on Diagnosis and Management. Gastroenterol Clin North Am 2016; 45:29–43 [PubMed: 26895679]
22. Tan Y, Schwartz LH, Zhao B. Segmentation of lung lesions on CT scans using watershed, active contours, and Markov random field. Med Phys 2013; 40:043502 [PubMed: 23556926]
23. Zhao B, Tan Y, Tsai WY, et al. Reproducibility of radiomics for deciphering tumor phenotype with imaging. Sci Rep 2016; 6:23428 [PubMed: 27009765]
24. Lin LI. A concordance correlation coefficient to evaluate reproducibility. Biometrics 1989; 45:255–268 [PubMed: 2720055]
25. E L, Lu L, Li L, et al. Radiomics for Classification of Lung Cancer Histological Subtypes Based on Nonenhanced Computed Tomography. Acad Radiol 2018;
26. E L, Lu L, Li L, et al. Radiomics for Classifying Histological Subtypes of Lung Cancer Based on Multiphasic Contrast-Enhanced Computed Tomography. J Comput Assist Tomogr 2019; 43:300–306 [PubMed: 30664116]

27. Peng H, Long F, Ding C. Feature selection based on mutual information: criteria of max-dependency, max-relevance, and min-redundancy. IEEE Trans Pattern Anal Mach Intell 2005; 27:1226–1238 [PubMed: 16119262]

28. Breiman L Random forests, machine learning 45. Journal of Clinical Microbiology 2001; 2:199–228

29. Esposito I, Konukiewitz B, Schlitter AM, et al. Pathology of pancreatic ductal adenocarcinoma: facts, challenges and future developments. World J Gastroenterol 2014; 20:13833–13841 [PubMed: 25320520]

30. Ganeshan B, Skogen K, Pressney I, et al. Tumour heterogeneity in oesophageal cancer assessed by CT texture analysis: preliminary evidence of an association with tumour metabolism, stage, and survival. Clin Radiol 2012; 67:157–164 [PubMed: 21943720]

31. Haralick RM, Shanmugam K, Dinstein IH. Textural features for image classification. IEEE Transactions on Systems Man & Cybernetics 2007; SMC-3:610–621

32. Ma Z, Fang M, Huang Y, et al. CT-based radiomics signature for differentiating Borrmann type IV gastric cancer from primary gastric lymphoma. Eur J Radiol 2017; 91:142–147 [PubMed: 28629560]

33. Yu H, Scalera J, Khalid M, et al. Texture analysis as a radiomic marker for differentiating renal tumors. Abdom Radiol (NY) 2017; 42:2470–2478 [PubMed: 28421244]

34. Canellas R, Burk KS, Parakh A, et al. Prediction of Pancreatic Neuroendocrine Tumor Grade Based on CT Features and Texture Analysis. AJR Am J Roentgenol 2018; 210:341–346 [PubMed: 29140113]

35. Zhu X, Dong D, Chen Z, et al. Radiomic signature as a diagnostic factor for histologic subtype classification of non-small cell lung cancer. Eur Radiol 2018; 28:2772–2778 [PubMed: 29450713]

1. Peng H, Long F, Ding C. Feature selection based on mutual information criteria of max-dependency, max-relevance, and min-redundancy. IEEE Transactions on pattern analysis and machine intelligence. 2005;27(8):1226–38. [PubMed: 16119262]

2. Breiman L Random forests. Machine learning. 2001;45(1):5–32.

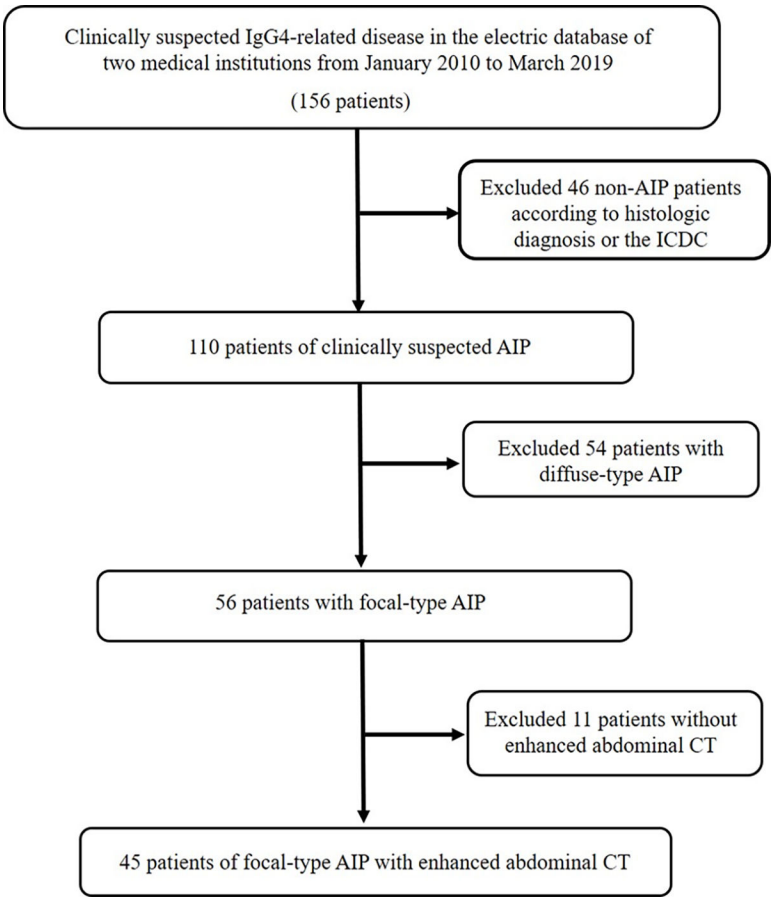

Figure. 1. Flow diagram of study population.

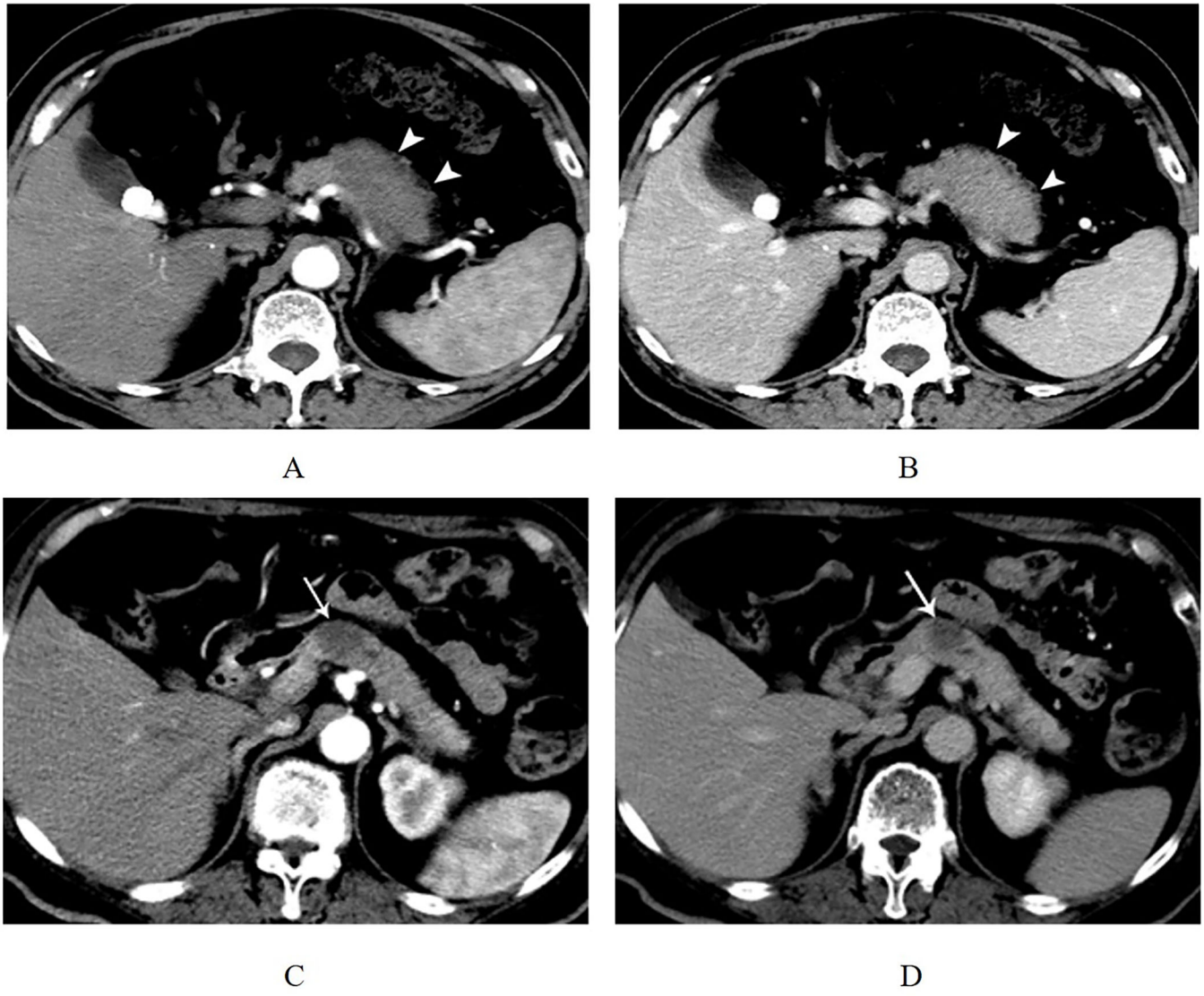

Figure. 2. Typical CT Features of focal-type autoimmune pancreatitis and pancreatic adenocarcinoma.

(A) A 63-year-old man with focal-type autoimmune pancreatitis. In arterial phase, the axial CT image shows a focal hypo-attenuation mass in the pancreatic body (white arrow head). (B) In venous phase, the focal mass of the pancreatic body shows the homogeneous enhancement and capsule-like rim (white arrow head). (C-D) A 49-year-old man who had abdominal pain for 1 year. Contrast-enhanced CT images show a 2 cm low-attenuation mass in the pancreatic neck in arterial and venous phases. The patient underwent surgery, and the final pathologic result was PDA (white arrow).

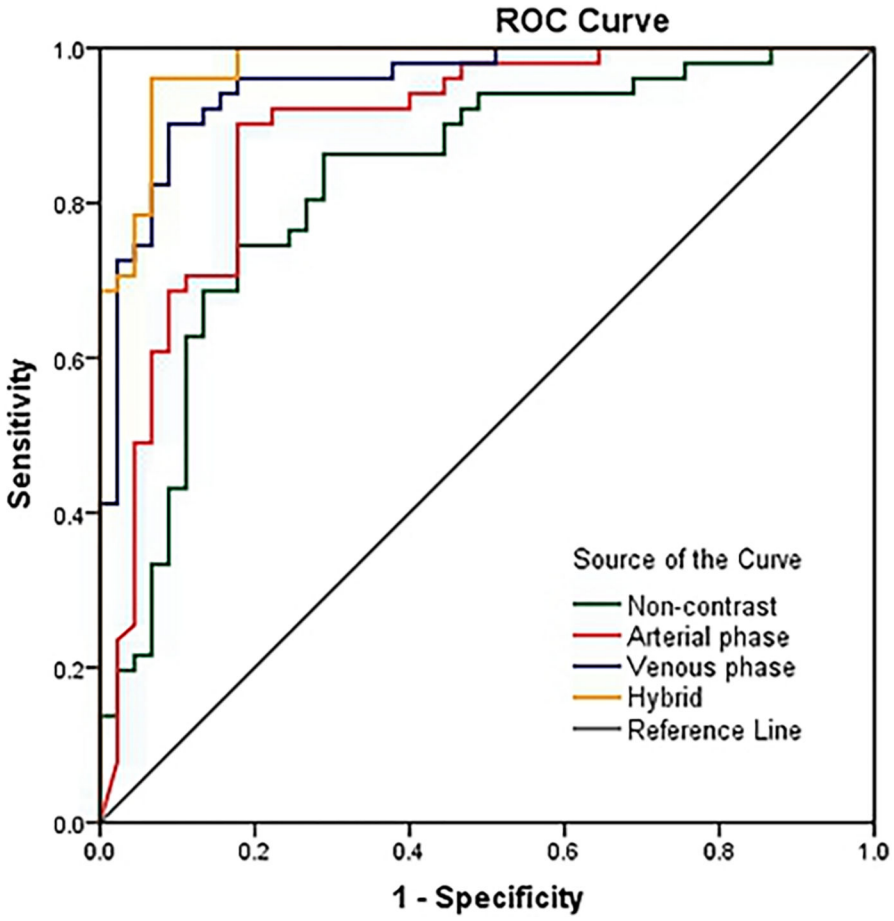

Figure. 3. Ability of receiver operating characteristic curves of the radiomics models to differentiate AIP and PDA.

The performances of radiomics models in differentiating AIP and PDA were AUC (95% CI) = 0.827 (0.737, 0.897), 0.890 (0.810, 0.945), 0.953 (0.890, 0.986) and 0.977 (0.924, 0.997) for the non-contrast, arterial phase, venous phase and hybrid of three phases, respectively. Variables in parentheses are not defined.

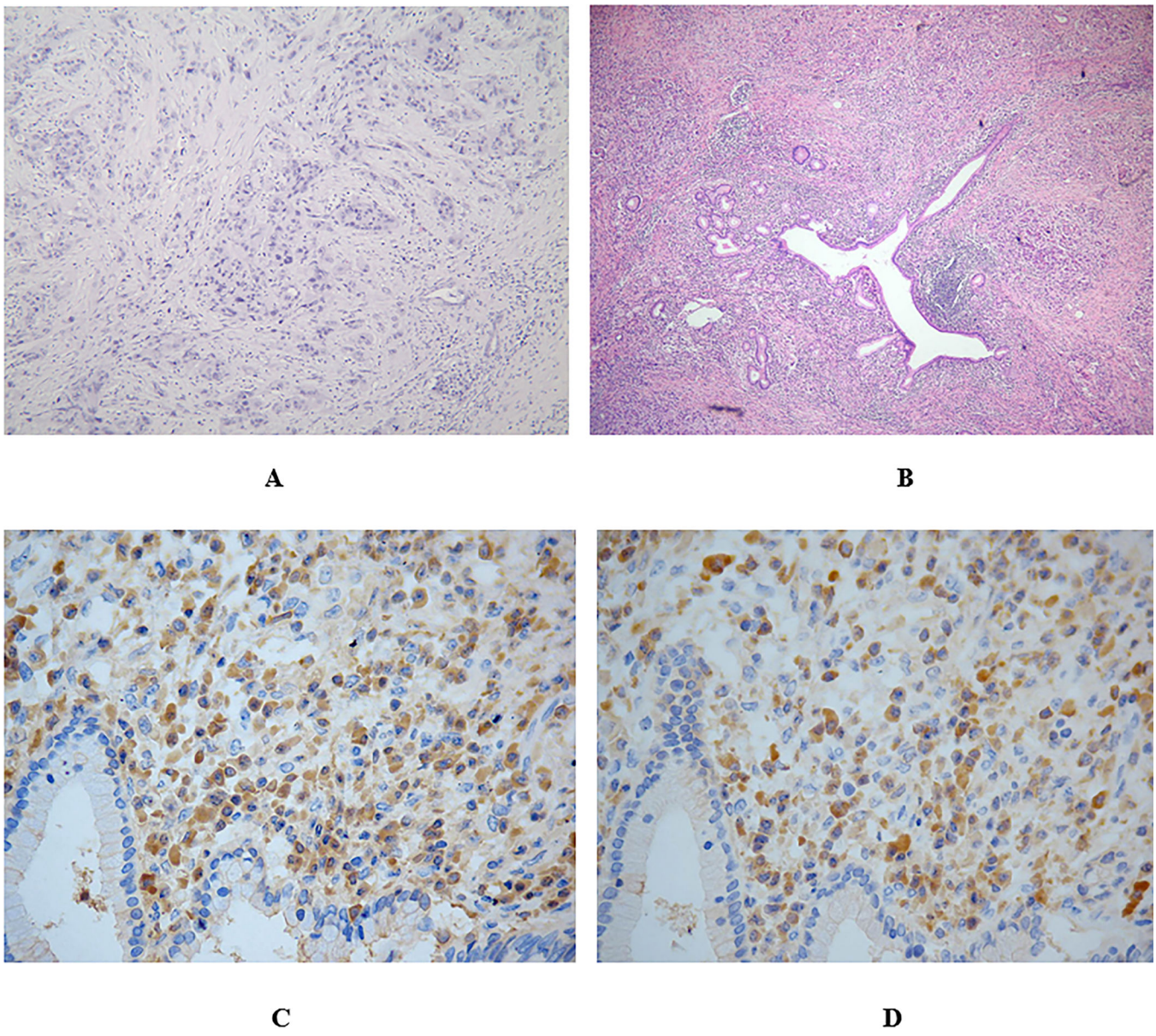

Figure. 4. Pathology of the PDA and AIP.

(A) Pathology of pancreatic adenocarcinoma. Note the haphazard arrangement of neoplastic cells and desmoplastic stroma (Hematoxylin and Eosin staining, original magnification × 100).

(B) Phomicrograph shows significant lymphoplasmacytic infiltration around pancreatic ducts with fibrosis (Hematoxylin and Eosin staining, original magnification × 100).

(C) Tissue was stained for IgG-positive cells.

(D) Tissue was stained for IgG4-positive cells .90% of IgG + plasma cells are IgG4 positive.

Table 1.

Patient Demographics and Clinical Features

	AIP (n=45)	PDA (n=51)	P
Age (range)	61 (34–78)	68 (45–83)	0.142
Gender			0.083
Male	26	38	
Female	19	13	
Clinical characters			
Weight loss	28	37	0.022
Abdominal pain	45	48	0.245
Jaundice	17	15	0.386
Laboratory data			
Elevated serum IgG4	27	0	
Elevated lipase	14	6	
Elevated CA19-9	15	32	
Surgery	3	27	
EUC-FNAB	11	8	

Note—Except for age, data are number of occurrences. Values in parentheses are range. Clinical information was not available for all patients.

IgG4 was measured in 38 patients with autoimmune pancreatitis, no patient with pancreatic ductal adenocarcinoma.

Lipase was measured in 45 patients with autoimmune pancreatitis, 21 patients with pancreatic ductal adenocarcinoma.

Cancer antigen 19-9 (CA 19-9) was measured in 45 patients with autoimmune pancreatitis, 51 patients with pancreatic ductal Adenocarcinoma.

EUC-FNA= endoscopic ultrasound guided fine needle aspiration biopsy

Table 2.

The ability of different approaches to differentiate AIP from PDA

AIP vs PDA	Sensitivity (%)	Specificity (%)	Negative Predictive Value (%)	Positive Predictive Value (%)	Accuracy (%)
Radiologist 1	57.78	90.20	80.70	66.67	75.00
Radiologist 2	73.33	88.24	78.95	84.62	81.25
Radiomics-Non-contrast	71.11	86.27	77.19	82.05	79.17
Radiomics-Arterial phase	82.22	90.20	85.19	88.10	86.46
Radiomics-Venous phase	93.33	96.08	92.00	89.13	90.63
Radiomics-Hybrid	93.33	96.08	94.23	95.45	94.80

Table 3.

Frequency of CT Imaging Feature

CT feature	AIP (n=45)	PDA (n=51)	p
Capsule-like rim	32 (71.11)	0	<0.001
Homogeneous enhancement in venous phase	41 (91.11)	0	<0.001
CT-attenuation values of pancreatic lesion (in HU), mean value ± SD			
Non-contrast	39.20 ± 5.81	33.85 ± 6.28	<0.001
Arterial phase	73.28 ± 19.31	44.10 ± 6.46	<0.001
Venous phase	81.47 ± 11.43	55.47 ± 10.14	<0.001
Extra-pancreatic			
Biliary dilatation	17 (37.78)	15 (29.41)	0.386
Vascular involvement (SMV, SMA, SPA, SPV)	19 (42.22)	33 (64.71)	0.027
Lymphadenopathy	11 (24.44)	16 (31.37)	0.451
Retroperitoneal stranding or fibrosis	2 (4.44)	0	0.217
renal involvement	5 (11.11)	0	0.020

Note--Data are in number of occurrences. Data in parentheses represent percentages.

AIP=autoimmune pancreatitis, PDA=pancreatic ductal adenocarcinoma.

SMV=superior mesenteric vein, SMA=superior mesenteric artery, SPA=splenic artery, SPV=splenic vein.

Table 4.

Selected features for creating radiomics models and their importance to the models

Non-Contrast		Arterial		Venous	
Features	**Importance**	**Features**	**Importance**	**Features**	**Importance**
LongRun-Low-GrayLevel-Emphasis	35%	LongRun-Low-GrayLevel-Emphasis	47%	LongRun-High-GrayLevel-Emphasis	45%
Intensity-Maximum	29%	LongRun-High-GrayLevel-Emphasis	36%	GLCM-Diff-Entropy	30%
LoG-Entropy	15%	Intensity-Kurtosis	9%	LoG-MGI	7%
Intensity-Root-mean-square	12%	GLCM-MCC	6%	GLCM-IMC2	7%
LoG-MGI	6%	Laws-10	1%	Laws-1	6%
Laws-1	4%	Laws-13	1%	Laws-13	4%